X-ray comb generation from nuclear-resonance-stabilized x-ray free-electron laser oscillator for fundamental physics and precision metrology

B. W. Adams and K.-J. Kim

Argonne National Laboratory, 9700 South Cass Avenue, Lemont, Illinois 60439, USA

(Received 16 August 2014; published 31 March 2015)

An x-ray free-electron laser oscillator (XFELO) is a next-generation x-ray source, similar to free-electron laser oscillators at VUV and longer wavelengths but using crystals as high-reflectivity x-ray mirrors. Each output pulse from an XFELO is fully coherent with high spectral purity. The temporal coherence length can further be increased drastically, from picoseconds to microseconds or even longer, by phase-locking successive XFELO output pulses, using the narrow nuclear resonance lines of nuclei such as ^{57}Fe as a reference. We show that the phase fluctuation due to the seismic activities is controllable and that due to spontaneous emission is small. The fluctuation of electron-bunch spacing contributes mainly to the envelope fluctuation but not to the phase fluctuation. By counting the number of standing-wave maxima formed by the output of the nuclear-resonance-stabilized (NRS) XFELO over an optically known length, the wavelength of the nuclear resonance can be accurately measured, possibly leading to a new length or frequency standard at x-ray wavelengths. A NRS-XFELO will be an ideal source for experimental x-ray quantum optics as well as other fundamental physics. The technique can be refined for other, narrower resonances such as ^{181}Ta or ^{45}Sc.

DOI: 10.1103/PhysRevSTAB.18.030711 PACS numbers: 06.20.F-, 41.60.Cr, 29.30.Kv, 76.80.+y

I. INTRODUCTION

X-ray quantum optics (XQO) is an emerging field offering perspectives ranging from fundamental physics to practical applications [1]. It builds upon the much more mature field of visible quantum optics at photon energies of a few eV and below [2]. However, beyond a mere repetition of already established techniques, XQO offers distinct advantages, such as the large photon energy for high-fidelity photon detection and the high photon momentum for matter-wave interferometry. Furthermore, keV-scale photons interact with matter differently from those at the eV scale, in particular, where nuclear resonance come into play. Nuclei resonant at x-ray energies, such as the well-known 5-neV-wide ^{57}Fe resonance at 14.4 keV, are ideal samples for XQO experiments, because they offer clean two-level systems with little dissipative coupling to the environment [1]. A good example are recent experiments done with ^{57}Fe nuclei in an x-ray resonant waveguide [3,4]. All experiments done to date with ensembles of such nuclei were in the single-photon regime because of limitations in the intensity and coherence length of state-of-the-art synchrotron light sources.

There is a wide range of XQO experiments that require higher intensities and higher degrees of coherence than the recent ones. Those include cases where x-ray coherent control of quantum states is required, such as going through part of a Rabi oscillation, stimulated Raman adiabatic passage techniques, etc. [1]. The x-ray free-electron-laser oscillator (XFELO) [5–8], if augmented by a stabilization of the cavity with an external x-ray frequency reference, can potentially fulfill these requirements.

When comparing different x-ray sources for their coherence and stability properties, there is a clear progression from tubes to storage rings to x-ray high-gain, single-pass free-electron lasers [9,10], then self-seeded Self-Amplified Spontaneous Emission (SASE) XFELs (SSS-XFEL) [11,12], and to the proposed XFELO, and, finally, to the nuclear-resonance-stabilized XFELO (NRS-XFELO) discussed here. Contemporary storage ring sources emit x rays into hundreds or thousands of transverse modes and, depending on the monochromator, typically thousands of longitudinal modes. The mode degeneracy, i.e., the number of photons per mode, is typically about 0.1–1.0. SASE XFELs emit about 10^{12}–10^{13} photons into a single transverse mode and hundreds of longitudinal modes. Self-seeding will reduce the number of longitudinal modes to a few, or even one, but some intensity fluctuations will remain. A SSS-XFEL can provide temporal coherence for pulses shorter than 0.1–1 ps, but there will be no coherence between pulses.

The output from an XFELO consists of pulses transmitted though the optical cavity each time the circulating, intracavity pulse hits one of the Bragg crystals, which is thin to transmit a few percent of the intracavity pulse. Each XFELO output pulse is fully coherent transversely as well as temporally. An XFELO pulse contains about

10^9 photons, smaller by 3–4 orders of magnitude compared to SASE. However, the XFELO repetition rate is much higher, and the intensity stability between pulses is also much higher than SASE, even with self-seeding.

A distinguishing feature of the XFELO is that the same pulse is recirculating, and identical copies of it are emitted from the cavity. *These output pulses are coherent with each other if the cavity length is kept stable.* The output spectrum then consists of a comb of sharp lines spaced at, typically, 10–20 neV from each other. If left to itself, however, the cavity length will fluctuate, and spontaneous-emission noise and other phase errors will also accumulate, so the comb lines will be effectively broadened up to their spacing, and interpulse coherence is lost. This can be prevented by locking the cavity length to an external reference to obtain an interpulse coherence commensurate with the stability of that reference. A convenient external reference is nuclear resonances, hence NRS-XFELO.

This paper is structured as follows: In Sec. II, we begin with an analysis of the spectrum of the XFELO output: It is a comb of lines spaced at the electron-bunch repetition rate, which is made equal to the cavity round-trip time. The frequency comb is offset from zero due to FEL gain effects. In Sec. III, we then propose a scheme to reference the frequency of one or more comb lines to a nuclear resonance line and to use a feedback loop acting on the cavity length to maintain resonance. Finally, Sec. IV briefly discusses some applications of such a frequency-stabilized XFELO.

II. THE COMB STRUCTURE OF AN XFELO AND TOLERANCE REQUIREMENTS

Consider now an ideal XFELO in the steady state. Electron bunches arrive at constant intervals T_e and meet the x-ray pulse circulating in the optical cavity at the undulator entrance. We designate one of the output pulses as the 0th one and write the electric field just outside the cavity as

$$E_0(t) = e^{i\omega_{\mathrm{FEL}}t}A(t). \tag{1}$$

Here ω_{FEL} is the frequency at the center of the XFELO bandwidth, and $A(t)$ is the envelope function, which we assume to be a Gaussian: $A(t) = A_0 \exp(-t^2/4\sigma_t^2)$. Here, σ_t is the rms duration of the radiation intensity $|A(t)|^2$. The $(n-1)$th pulse is from the intracavity pulse after circulating n times, and its wave form is therefore displaced by n round-trip periods. However, we should pay attention to the fact that the round-trip periods of the pulse envelope and the pulse phase are, in general, different. The round-trip period for the phase is given by $T_{\mathrm{ph}} = T_c + \Delta\varphi/\omega_{\mathrm{FEL}}$, where $T_c = L/c$ is the round-trip time of the phase absent any FEL interaction and $\Delta\varphi$ is the phase delay due to the index of refraction of the FEL interaction [13]. The latter in radians is approximately equal to the value of the incremental gain, which is small (<0.2) and, to the first order, independent of both T_{ph} and the electron-bunch recurrence interval T_e. We will therefore neglect it and simply write $T_{\mathrm{ph}} = T_c$ in the following. The round-trip period of the pulse envelope is the same as electron-bunch spacing T_e in steady-state operation and should be slightly longer than T_c to compensate for the lethargy effect arising from the fact that the later part of the x-ray pulse receives more amplification [14]. For FEL gain to be effective, we must require that the electron bunches overlap with the recirculated x-ray pulses well within the bunch duration, i.e.,

$$|T_e - T_c| \ll \sigma_t. \tag{2}$$

Assuming for now a constant T_c, i.e., a perfectly stable cavity and the absence of other phase noise to be discussed below, we see that the electric field of the nth pulse is given by

$$E_n(t) = e^{-i\omega_{\mathrm{FEL}}(t-nT_c)}A(t-nT_e). \tag{3}$$

The electric field for the sum of N pulses in frequency representation is

$$\begin{aligned}\tilde{E} &= \frac{1}{\sqrt{2\pi}}\int dt e^{i\omega t}\sum_{n=0}^{N-1}E_n(t)\\ &= \left(\sum_{n=0}^{N-1}\exp\{in[\omega T_e - \omega_{\mathrm{FEL}}(T_e - T_c)]\}\right)A(\omega-\omega_{\mathrm{FEL}}),\end{aligned} \tag{4}$$

where $A(\omega-\omega_{\mathrm{FEL}}) = \tilde{A}_0\exp[-(\omega-\omega_0)^2/4\sigma_\omega^2]$ is the FEL spectral envelope with a transform-limited bandwidth satisfying $\sigma_t\sigma_\omega = 1/2$. The first factor in Eq. (4) gives rise to a comb structure for large N, with teeth located at

$$\omega = \omega_{\mathrm{FEL}}\frac{T_e - T_c}{T_e} + \frac{2\pi}{T_e}n, \tag{5}$$

where $n = 0, \pm1, \ldots, 2, \ldots$. However, due to the spectral envelope $A(\omega-\omega_{\mathrm{FEL}})$, only frequencies ω near ω_{FEL} are relevant, which are given by $n \approx n_{\mathrm{FEL}}$, where

$$n_{\mathrm{FEL}} = \frac{\omega_{\mathrm{FEL}}T_c}{2\pi} \tag{6}$$

is the number of x-ray wavelengths that fit into the cavity length L. Then Eq. (5) can be written as

$$\omega = \omega_{\mathrm{FEL}} + \frac{2\pi}{T_e}(n - n_{\mathrm{FEL}}). \tag{7}$$

The requirement that n_{FEL} be an integer, together with a nominal design value for T_c, fixes the value of ω_{FEL}.

For an electron-bunch recurrence rate of, say, 3 MHz, the teeth are spaced at 14 neV while the spectral envelope is of the order of 3 meV wide. There are, thus, several hundred

thousand teeth in the comb. Note the similarity of Eq. (5) with that occurring in a mode-locked optical laser [15].

In a practical situation, the radiation spectrum fluctuates due to a number of noise sources, in particular, cavity-length fluctuations, spontaneous undulator emission, and jitter in the electron-beam properties and arrival times. Rapid (on the scale of T_e) and strong fluctuations lead to a broadening of the comb lines up to the point where the lines merge, and the comb is destroyed. This will be explored in more detail in Sec. III B. Here, we will concentrate on the effect of slower and weaker fluctuations on the spectrum, which are due to fluctuations δT_c and δT_e of T_c and T_e in Eq. (5). All noise causing spectral change can be mapped onto these two. Figure 1 shows qualitatively how these two affect the comb spectrum. A small, sub-Ångström change in the cavity length, and thus a subattosecond change in the round-trip time T_c, will shift the entire comb, and a change in the electron-beam repetition rate will change the relative spacing of the comb lines.

The tolerances on the fluctuations δT_c and δT_e are determined by the following condition:

$$|\delta\omega| = \left|\delta\omega_{\mathrm{FEL}} - 2\pi\frac{\delta T_e}{T_e^2}(n - n_{\mathrm{FEL}})\right| \ll \frac{2\pi}{T_e}. \qquad (8)$$

Assuming uncorrelated fluctuations δT_c and δT_e, this leads to two conditions. First,

$$|\delta\omega_{\mathrm{FEL}}| = \left|\tfrac{\delta T_c}{T_c}\omega_{\mathrm{FEL}}\right| = \left|\tfrac{c\delta T_c}{T_c}\tfrac{2\pi}{\lambda_{\mathrm{FEL}}}\right| \ll \tfrac{2\pi}{T_c} \rightarrow \tfrac{\delta L}{\lambda_{\mathrm{FEL}}} \ll 1. \qquad (9)$$

Here δL is the cavity-length fluctuation. Second,

$$\begin{aligned} &\left|\frac{\delta T_e}{T_e}(n - n_{\mathrm{FEL}})\right| \ll 1 \\ \rightarrow &\left|\frac{\delta T_e}{\sigma_t}\frac{(n - n_{\mathrm{FEL}})}{\sigma_n}\frac{\sigma_t\sigma_\omega}{2\pi}\right| \ll 1 \\ \rightarrow &\left|\frac{\delta T_e}{\sigma_t}\frac{(n - n_{\mathrm{FEL}})}{\sigma_n}\frac{1}{4\pi}\right| \ll 1. \end{aligned} \qquad (10)$$

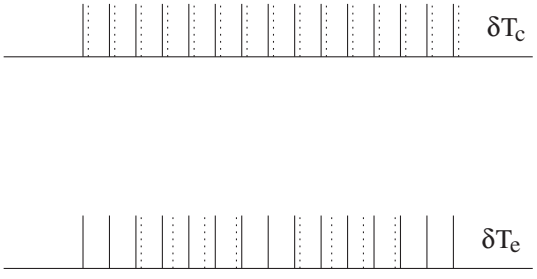

FIG. 1. Illustration of the effects of fluctuations in T_c and T_e in Eq. (5) on the comb spectrum. A change in T_c will shift the entire comb, and a change in T_e will change the spacing of the comb lines.

In the above, σ_ω is the rms FEL bandwidth, and $\sigma_n = (T_e/2\pi)\sigma_\omega \approx (T_e/2\pi)\sigma_\omega$ is the corresponding spread of the comb-line numbers. In the last step, we used the fact that $\sigma_t\sigma_\omega = 1/2$ for a Gaussian coherent pulse. The last inequality in Eq. (10) is not difficult to satisfy; for $\sigma_t \ll 0.5$ ps, we can set $\delta T_e \leq 5$ fs and $|(n - n_{\mathrm{FEL}})/\sigma_n| \leq 0.1$, and the left-hand side of the last inequality becomes less than 10^{-4}. The fact that the tolerances on the electron-bunch period on the spectral comb are much more relaxed compared to that on the phase period could have been anticipated from the fact that the electron pulse period enters in the pulse envelope rather than the pulse phase, as described by Eq. (3).

Having seen that the tolerance on the electron-bunch period is manageable, let us discuss qualitatively the tolerances in the fluctuations of other electron-bunch properties, such as energy, energy chirp, energy spread, electron beam emittance, etc. These lead to a fluctuation in the complex gain of the electric field. The fluctuation in the real part is not expected to play a significant role in the spectral comb fluctuation, because it does not directly influence the phase of the electromagnetic field. The fluctuation in the imaginary part will have a direct influence on the spectral position. For the low-gain regime in which an XFELO operates, the magnitude of the imaginary part is of the same order as the real part [13]. With a power gain of 0.2, i.e., an amplitude gain of 0.1, and an estimated fluctuation in this number of 1%, the phase fluctuation would be 10^{-3} rad, which is negligible. We expect that advances in electron-accelerator technology will permit a further reduction of the gain fluctuation by a factor of 10. At that point, and with the machine parameters assumed for this study, the phase fluctuations from spontaneous undulator emission become dominant (see below). We will therefore focus our attention to the fluctuations of the x-ray cavity.

III. CAVITY STABILIZATION

A. Schematic

Even if fluctuations in cavity length and electron-beam parameters are small enough to yield well-defined comb lines, these will drift over time [for the distinction between line broadening and drift or jitter, see remarks after Eq. (16)]. The comb will then be smeared out to eventually cover the entire spectrum within the envelope $\tilde{A}(\omega - \omega_0)$. This drift can be prevented by locking one (or more; see below) comb line to a reference that is not subject to drift. At x-ray frequencies, such references are found in nuclear resonances. Figure 2 shows schematically how the cavity stabilization may be done. A nuclear-resonant sample (here ^{57}Fe) is placed in the XFELO output beam, and the nuclear resonance fluorescence and inner-shell electronic fluorescence at 6 and 7 keV are monitored as a measure of how close one of the XFELO longitudinal modes is to the

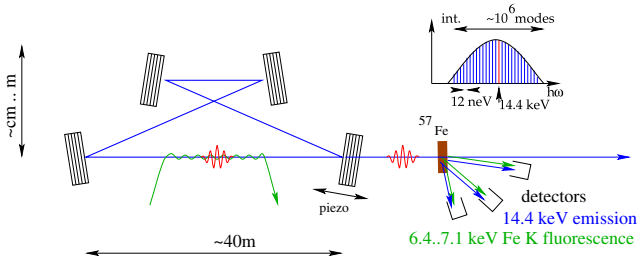

FIG. 2. Schematic of the cavity-stabilization scheme. A nuclear-resonant sample (here ^{57}Fe) is placed into the XFELO output, and the nuclear-resonant and K-shell electronic fluorescence are monitored as a function of cavity tuning with a piezoelectric actuator. A feedback loop keeps one of the ca. 10^6 longitudinal modes of the XFELO on resonance with the sample.

resonance. By scanning the cavity length over one x-ray wavelength (0.86 Å for ^{57}Fe), the comb is shifted by the spacing of its lines, and the maximum of the nuclear-resonant response is found within the scan. The contrast, i.e., the height and inverse width of the response peak, depends on how many x-ray pulses interact with the nuclei during their resonant lifetime and how much the x-ray-pulse phase fluctuates. If all pulses are in phase to reinforce nuclear-resonant oscillations from previous pulses, then the response is strongest. We will show in Sec. III B that this effect can be expressed by the parameter $\Lambda = \sigma^2 + \Gamma T_e$, where σ is the rms uncorrelated phase noise and Γ is the resonant linewidth. Figure 3 shows the absorption rate of resonant nuclei in such a cavity scan for several values of Λ. Once the maximum resonance-fluorescent response of the NR sample is found, a feedback loop can maintain it.

In a specific XFELO example with an $L = 90$-m round-trip cavity, the comb lines are spaced at $\Delta E = 14$ neV from each other. A single x-ray pulse has an rms duration of about $\sigma_t = 500$ fs corresponding to the transform-limited FWHM energy bandwidth of 1.6 meV. For $T = 300$ ns and

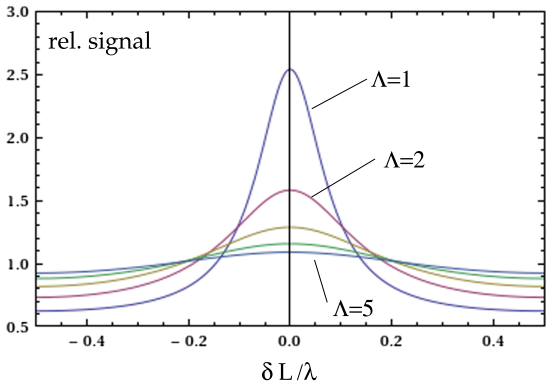

FIG. 3. Resonant-fluorescent response in a scan of the cavity length L over one x-ray wavelength λ for values of $\Lambda = 1, 2, 5$ (introduced in Sec. III B). The signal is relative to the case without cavity modulation of the spectrum.

an ideal bandwidth $\Gamma = 4.7$ neV, $\Gamma T/h = 2.14$. Even taking into account some inhomogeneous line broadening to about 8 neV, $\Gamma T/h = 3.64$, and the fluorescent response can resolve the 14-neV mode spacing of the NRS-XFELO. The sample in Fig. 3 should be sufficiently thick to intercept enough photons for a strong signal yet still optically thin enough to suppress superradiant line broadening. At an optical thickness of 0.1 and 10^9 photons per pulse in 10^6 longitudinal modes (teeth of the comb), the sample will absorb about 100 photons per pulse and will emit close to that number into 4π as 14.4-keV photons (a fraction of about 11%) and Fe fluorescence (89%). In order to measure the fluorescent response at an accuracy of 1%, one then needs to collect the signal from 100 pulses (assuming Poisson statistics). At a pulse repetition rate of 3 MHz, this means that the signal can detect deviations from the resonant condition at frequencies up to $f_{\mathrm{FB}} \approx 30$ kHz.

Several approaches for feedback making use of the fluorescence signal will be possible. One approach is the null-detection feedback technique employed at the Laser Interferometer Gravitational-Wave Observatory (LIGO) in which the fluorescence signal is processed while one of the XFELO Bragg mirrors is given a small-amplitude oscillation [16]. The method was successfully tested in a pilot experiment with a high-resolution, six-crystal x-ray monochromator at APS Sector 30 [17]. Another approach is to use the signal from multiple longitudinal modes by moving several samples at velocities in multiples of about 0.3 mm/s. As is well known in the Mössbauer-spectroscopy community, this velocity introduces a Doppler shift equal to the 14-neV mode spacing. With this technique, one can both increase the signal strength, and thus improve the bandwidth of the feedback loop, and avoid the non-Doppler-shifted mode altogether to leave it for experiments with stabilized radiation. Furthermore, samples can be Doppler-shifted to frequencies slightly above and below a resonance to obtain sign information for the feedback loop by taking the difference of their signals. This is shown schematically in Fig. 4. This technique of using multiple comb lines can also be used to speed up the response of the feedback loop with very long-lived isotopes, such as ^{45}Sc (300 ms lifetime) whose

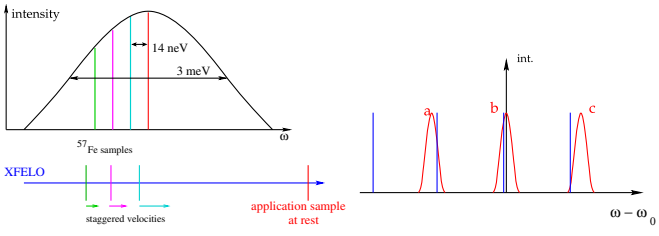

FIG. 4. Using the Doppler shift on multiple samples (left) to increase the signal strength and (right) to obtain a sign signal for the feedback in addition to the maximum signal.

response is intrinsically slower than the above value of $1/f_{\mathrm{FB}} \approx 30\ \mu$s. In such cases, one may exploit the effect of superradiant line broadening for a faster response [18] and use several samples of different optical thickness, i.e., different amounts of line broadening, on different comb lines.

B. Sources of phase noise

Radiation coming from a nonideal XFELO will exhibit amplitude fluctuations. In steady-state operation, these are constrained in modulus but not in phase. The phase noise can be described by replacing Eq. (3) with

$$E_n(t) = e^{i\psi_n} e^{-i\omega_{\mathrm{FEL}}(t-nT_c)} A(t-nT_e). \tag{11}$$

The random phases $\psi_n = \phi_n + \varphi_n$ are modeled here as sums of two contributions: The first comes from singular random phases ϕ_n that affect each pulse separately. These may be due to uncorrelated noise outside of the XFELO cavity. The second contribution comes from persistent phase jumps $\varphi_n - \varphi_{n-1}$ that add up to the phase φ_n in the nth pulse. The most important contribution to this type of noise comes from spontaneous undulator emission that is superposed on the FEL emission. The superposition amplitude is recirculated into the FEL, and therefore the phase jumps are persistent.

This discussion does not consider cavity-length fluctuations that may be caused by thermal expansion of the cavity mirrors due to x rays absorbed in them. That heat load is pulsed and occurs at the very well-defined cavity round-trip frequency. Stochastic variations enter only through fluctuations of the circulating x-ray power, which can be stabilized in a feedback loop. Furthermore, the thermal expansion can be brought to the 10^{-9}/K level by cryocooling the diamonds [19,20], and heat conduction is greatly improved by the use of isotopically pure diamond, as is standard in the electronics industry. These issues must be left to a detailed engineering study.

Equation (4) for the frequency representation of the electric field can now be adapted to accommodate the phase errors. Equation (4) now becomes

$$\begin{aligned}\tilde{E} &= \frac{1}{\sqrt{2\pi}} \int dt e^{i\omega t} \sum_{n=0}^{N-1} E_n(t) \\ &= \left(\sum_{n=0}^{N-1} \exp\left[in\omega T_c + \psi_n \right] \right) A(\omega - \omega_{\mathrm{FEL}}).\end{aligned} \tag{12}$$

The ensemble average of the intensity from N pulses is then

$$\langle |\tilde{E}(\omega)|^2 \rangle = NU |\tilde{A}(\omega - \omega_{\mathrm{FEL}})|^2, \tag{13}$$

where

$$U = 1 + \frac{1}{N} \left\langle \sum_{n \neq m} e^{i\omega(n-m)T_c} e^{i(\psi_n - \psi_m)} \right\rangle. \tag{14}$$

This function U can be evaluated by using the approximations of Gaussian-distributed phase noise with uncorrelated contributions at different time constants. The calculation shown in Appendix A yields Eq. (A17):

$$\begin{aligned}U = &\frac{\sinh(\sigma^2/2)}{\sinh^2(\sigma^2/4) + \sin^2(\omega T/2)} \\ &+ \frac{1 - \cosh(\sigma^2/2)\cos(\omega T) + e^{-N\sigma^2/2} C_N(\sigma^2/2, \omega T)}{4N[\sinh^2(\sigma^2/4) + \sin^2(\omega T/2)]^2},\end{aligned} \tag{15}$$

where C_N is given by Eq. (A14).

The function U peaks at frequencies ω for which ωT is an integer multiple of 2π. Although the full expression for the spectral shape is rather complicated, it becomes much simpler in the limiting cases of $N\sigma^2/2 \gg 1$, where the first fraction in Eq. (15) is dominant, and $N\sigma^2/2 \ll 1$, where the second fraction is dominant. These two cases correspond to comb-line broadening vs line jitter: In the absence of noise, the lines would sharpen up as more and more pulses are added. The noise limits this sharpening as the phase diffuses away while further pulses are added. Thus, the natural linewidth is equal to the free spectral range ω_T divided by N_n^2, where $N_n\sigma/2 = 1$. As further pulses are added, the linewidth will stay at that value, and the center of the line will diffuse due to noise. For $N\sigma^2/2 \ll 1$ (dominant 2nd fraction),

$$U \approx \frac{1}{N} \left(\frac{\sin(\pi N \Delta\omega/\omega_T)}{\sin(\pi \Delta\omega/\omega_T)} \right)^2, \tag{16}$$

where $\omega_T = 2\pi/T_c$ and $\Delta\omega$ is the difference of ω from the closest integer multiple of ω_T. For $N\sigma^2/2 \gg 1$ (dominant F_1), but $\sigma^2/4 \ll 1$, and ωT_c close to an integer multiple of 2π, the function U approximates a Lorentzian:

$$U \approx \frac{\sigma^2/2}{(\sigma^2/2)^2 + (\pi\Delta\omega/\omega_T)^2}. \tag{17}$$

With typical values of $\sigma^2 = 10^{-8}$ (spontaneous emission only), and $\omega_T = 3$ MHz, the linewidth is about 10^{-12} eV.

Now to the response of a resonant nucleus to the XFELO radiation: The scattering or absorption form factor of a nucleus is [21]

$$f_0 = \frac{\Sigma_a c \omega_R}{4\pi} \frac{\Gamma/2}{\omega - \omega_0 - i\Gamma/2}, \tag{18}$$

where Γ is the resonant linewidth. Nuclear resonances have linewidths in the micro-eV down to atto-eV range,

i.e., much less than the milli-eV XFELO bandwidth. Γ may be smaller or larger than the width of one peak in Eq. (17). Σ_a is the absorption cross section at the resonance wavelength λ_R:

$$\Sigma_a = \frac{\lambda_R^2}{2\pi}\frac{2I_e+1}{2I_g+1}, \tag{19}$$

where I_g and I_e are the angular momenta of the ground and excited states, respectively. For ^{57}Fe, $I_g = 3/2$ and $I_e = 5/2$. The resonant scattering or absorption amplitude is then found by multiplying Eq. (11) with (18). This leads to the absolute square of Eq. (18) in Eq. (14). The number of scattered or absorbed photons is then found by integrating over the photon phase-space density $d^3n_\gamma/d^2x d\omega$, where dn_γ is the number of incident photons in a cross section d^2x and a frequency interval $d\omega$. Then, we need to calculate integrals of the type

$$\int_{-\infty}^{\infty} \frac{e^{i\omega A}}{(\omega-\omega_R)^2+(\Gamma/2)^2}\,d\omega = \frac{2\pi}{\Gamma}\,e^{i\omega_R A-\Gamma|A|/2} \tag{20}$$

with $A = (n-m)T_c$. This result can be carried through the steps leading to (16) and (17) where σ^2 is replaced with $\Lambda = \sigma^2 + \Gamma T_c/2$.

An explicit calculation of σ requires a model for the cavity-length fluctuations. These depend on the mechanical design of the mirror mounts and how well local machinery is isolated. A rough estimate can be found in an empirically determined formula for seismic noise developed in the context of laser-interferometric gravitational-wave detectors [22]:

$$\frac{\Delta L^2[\mathrm{m}^2]}{\Delta f[\mathrm{Hz}]} = 10^{-18}\left(\frac{10\ \mathrm{Hz}}{f}\right)^4 \equiv G(f). \tag{21}$$

To find the variance of the cavity-length fluctuations $\delta x_{k,q}$ that enter the phases $\phi_{k,q}$ in Eq. (A2), we need to integrate over the frequency interval $1/qT \ldots 1/(q+1)T$ attributed to those fluctuations:

$$\langle \delta x_q^2\rangle = G(1/qT)\left(\frac{1}{qT}-\frac{1}{(q+1)T}\right). \tag{22}$$

With $\sigma_q^2 = 4\pi^2\langle\delta x_q^2\rangle\lambda^2$, this can now be inserted into Eq. (A3) to yield

$$\langle(\psi_n-\psi_m)^2\rangle = \frac{4\pi^2(n-m)}{\lambda^2}\sum_{q=1}^{(n-m)/2}\frac{qG(1/qT)}{q(q+1)T}. \tag{23}$$

Insertion of the numerical values of Eq. (21), and with $\lambda = 0.86$ Å and $T = 300$ ns, yields $n-m \approx 140$ for a phase fluctuation of 1%. Thus, the feedback loop has to have a bandwidth of 3 MHz/140 $\approx$ 24 kHz to maintain a stable phase.

IV. APPLICATIONS

A NRS-XFELO will find numerous applications in highly precise metrology and fundamental-physics studies. Key to this prospect is that nuclear resonances offer clean and well-isolated two-level quantum systems. Furthermore, nuclear resonances have rather large absorption and scattering cross sections of the order of the wavelength squared. This is much larger than the nonresonant electronic scattering cross section of the classical electron radius squared. Within the narrow linewidth of the respective resonant isotope, nuclear-resonant processes thus far outweigh the competition from electronic scattering or photoelectric absorption. Stabilization of the XFELO is necessary to make full use of that dominance. Even so, the raw output of the XFELO contains about a million comb lines of which only a few are relevant for nuclear-resonant experiments. For some of the applications, it may be necessary to remove the non-nuclear-resonant radiation in the XFELO output to minimize disturbances. This can be done by use of a spectral converter comprised of a nuclear-resonant foil at about unity optical thickness and a chopper to remove the radiation pulses, as discussed in Sec. IV B.

The metrology for improved time and length standards shall now be discussed in more detail in Sec. IV A, followed by a discussion of a few fundamental-physics applications in Sec. IV C.

A. Time and length standard

Nuclear resonances are typically extremely sharp and thus hold great potential as time and length standards. A NR-XFELO would be an intense source of very narrow-band radiation for use in metrology. The isotope ^{45}Sc with a 10^{-15}-eV linewidth of a resonance at 12.4 keV would match the natural linewidth of an XFELO with the above parameters for an accuracy of 10^{-19}, and other isotopes, such as ^{103}Rh (39.8 keV, 1.35×10^{-19} eV), may improve this even further. This is several orders of magnitude better than current atomic clocks. To fully make use of such an ultrastable x-ray reference, one has to tie the x rays to optical-wavelength standards. This can be done interferometrically, as first proposed by Shvyd'ko [23]. In that concept, a pair of sapphire crystals forms a Fabry-Perot interferometer simultaneously for x rays and for visible light. To count x-ray fringes, the fluorescence response of resonant nuclei would be monitored, which respond only to a narrow-band section of a potentially much broader incident spectrum from, e.g., a synchrotron radiation source. In a centimeter-long scan, about 10^8 x-ray fringes and 10^4 optical ones are counted. To reach an accuracy of 10^{-12}, corresponding to the natural linewidth of ^{57}Fe, one would then have to interpolate 10^4-fold for the x rays and

10^8-fold for the optical interference, i.e., measure intensities at points in increments of 10^{-14} m.

A NRS-XFELO with its highly collimated intense output of frequency-stable radiation offers a way of achieving the same accuracy with significantly relaxed requirements on the resolution: by scanning a standing x-ray wave over a distance of, say, 10 m, an accuracy of 10^{-12} can be reached in steps of 10^{-11} m, i.e., by interpolating tenfold between x-ray fringes, and 10^5-fold between optical fringes, respectively. The latter is state of the art with industrial heterodyne interferometers [24,25]. The highly collimated, single-transverse-mode output of an XFELO is needed in this scheme to eliminate geometric path errors over the 10-m scan range. Nuclear-resonant cavity stabilization of the XFELO is required to avoid jumping of modes leading to miscounts of fringes. Furthermore, with isotopes exhibiting narrower resonances than ^{57}Fe, the cavity stabilization is essential to keep the radiation on resonance all the time, and not just a fraction statistically proportional to the ratio of resonant linewidth to cavity-mode spacing (here, 14 neV).

Figure 5 shows a possible implementation with an assembly of two x-ray-focusing Fresnel zone plates and a single nucleus of ^{57}Fe embedded in a host crystal of light elements (diamond or beryllium metal) traveling along a 10-m-long standing-wave field generated by backreflection of the output from a NR-XFELO. The distance of this assembly from the backreflecting mirror is measured optically to 10^{-11} m, which is possible with commercial heterodyne interferometers. The left-hand zone plate focuses the incident beam to 50 nm, and the right-hand one recollimates it and then focuses the returning beam. With an absorption cross section of 10^{-22} m^2 [26] and a flux of 10^3 resonant photons per pulse repeating at 3 MHz, a single ^{57}Fe nucleus in that focus will absorb a few thousand photons per second for a reasonably strong signal. Using a single nucleus eliminates inhomogeneous broadening, which is especially important for isotopes with narrower resonances than ^{57}Fe. Sparse sampling using preexisting knowledge of the resonant wavelength can be employed to significantly reduce the number of fringes to be counted. For narrower-line isotopes, the scan could be extended to cover, say, 1 km. As long as the cavity stabilization is maintained, the signal from the narrow-line nucleus is of the same order of magnitude as that from ^{57}Fe, because the resonant absorption cross section of all these two-level transitions is of the order of λ^2.

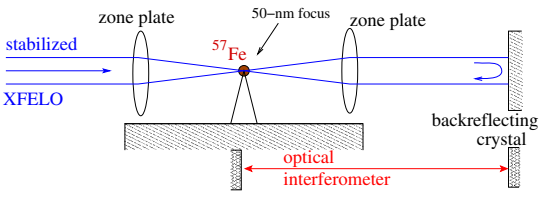

FIG. 5. Schematic depiction of how to probe a meter-to-kilometer-long x-ray standing-wave field while comparing to an optical length standard. Two Fresnel zone plates generate a 50-nm x-ray focus that travels along the standing waves. A single ^{57}Fe nucleus in the focus senses the standing-wave intensity through resonance fluorescence.

B. Spectral conversion

Even with stabilization, only about a fraction of 10^{-6} in the XFELO output is resonant (without stabilization, it may well be much less, as comb lines hit a resonance only occasionally). This may be a problem in some applications where electronic absorption and scattering may overshadow resonant effects. In such cases, a spectral converter can be used, which is based on the effect of coherent nuclear-resonant forward scattering. This device is shown schematically in Fig. 6. A nuclear-resonant foil of about unit optical thickness is placed into the beam path, and an x-ray chopper further downstream removes the radiation pulses transmitted through the foil (the so-called prompt pulses) while allowing passage of radiation for a large fraction of the remaining time. As is well known from time-domain Mössbauer spectroscopy, the foil reradiates long wave trains given by the reciprocal resonant linewidth. These go into the same spatial mode as the incident beam and are coupled coherently to it. Stabilization of the XFELO ensures that these wave trains are coherent with each other or, for resonant lifetimes that are longer than the pulse repetition period, that the wave train does not undergo phase jumps. The radiation after the chopper is then reduced in average intensity, but all of it is resonant. In effect, a single line is singled out from the comb, or a few in case the comb spacing matches Zeeman splitting in the foil.

In order to handle the high heat load of the XFEL output, the chopper should be designed to deflect the prompt pulses onto a beam stop instead of directly absorbing them. This might be done by using a spinning crystal, Bragg-reflecting micromechanical device, or surface-acoustic-wave device.

C. X-ray quantum optics

As mentioned in the introduction, x-ray quantum optics offers interesting new fields in x-ray science and opens new possibilities in the study of fundamental physics. On the one hand, techniques and ideas can be taken from conventional quantum optics to find analogues in the x-ray regime for higher-resolution spectroscopy, lower radiation exposure of samples, etc. On the other hand, x rays offer much more than an extension of existing techniques: (i) The large

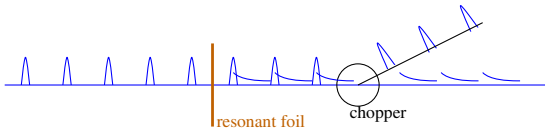

FIG. 6. Schematic of a spectral converter to isolate a single comb line.

photon energy permits low-noise, high-fidelity photon detection, for example, to close loopholes in tests of quantum physics using entangled photons; (ii) the large photon momentum permits the manipulation of matter, for example, in matter-wave interferometry or experiments on entanglement of photonic and mechanical-vibration modes [27]; (iii) x rays interact with inner-shell electrons and outer-shell orbitals; (iv) unlike eV-scale light, which interacts with matter only through the electrons, x rays can also excite nuclear isomer states. Finally, (v) x-ray energies approach the pair-creation threshold of 2×511 keV, where the quantum vacuum itself changes its character. Because of the uncertainty relation, effects of this threshold may appear at energies well below 1 MeV. Especially attractive for quantum optics is the use of nuclear resonances, because these offer clean two-level interactions with very little decoherence from coupling to other degrees of freedom. One may even observe spontaneously generated coherence [28].

The high, resonantly tuned photon flux out of a NRS-XFELO brings a number of x-ray quantum-optical experiments into the realm of the feasible [29]. Although a detailed discussion would go beyond the scope of this text, and a lot of design work remains to be done, a few salient points can be mentioned here: In matter-wave interferometry using eV-scale laser light for splitting beams of atoms or molecules, the photon momentum is insufficient for splitting beams to angles large enough that they become physically separated by more than their diameters. Here, the roughly 10 000 times higher momentum of x-ray photons will help to macroscopically separate the beams. Electronically excited states at x-ray energies are far too short-lived to be useful for such experiments, and even among nuclear resonances, longer-lifetime ones such as ^{45}Sc will have to be used. It is then essential to use a NRS-XFELO both to stay on resonance and to ensure coherence times long enough to cover coherence over travel times of the matter in the interferometer. Even then, the above resonant cross section will make matter-wave interferometry difficult, and one may have to resort to additional measures, such as an external resonant build-up cavity (or place the experiment inside the XFELO cavity), and/or a high-gain single-pass XFEL as an "afterburner" seeded by a NRS-XFELO.

Another study that may become feasible with a NRS-XFELO is the study of the size dependence of quantum decoherence using mesoscopic pieces of matter in optical traps [30]. In this proposal, a UV laser beam is to be used to locate a 100-nm-size object cooled to its vibrational ground state in an optical trap and to generate a Schrödinger-cat state for the case that no laser light is scattered. In such an experiment, one could achieve a much sharper localization if, instead of scattering UV light off a glass sphere, one were to scatter nuclear-resonant x rays off a nanoparticle core at the center of the sphere. The entire sphere is then located by measuring at its center. Nuclear-resonant scattering will be clearly distinct from Thomson scattering due to its much higher cross section, as well as the time delay. A NRS-XFELO would be required for this experiment in order to obtain certainty of localization from a high, on-resonant photon flux.

Yet another interesting application of a NRS-XFELO would be the possibility to create high-photon-number Fock states by scattering the x rays off nanoparticles of nuclear-resonant material and to velocity select between absorption and reemission. One can then even think of creating entangled states at high, but clearly defined photon numbers, the so-called high-noon states [31–33] [a pun on the notation $(|N\rangle|0\rangle + |0\rangle|N\rangle)$]. These are of fundamental interest and have applications in measurements that beat the wavelength resolution limit.

V. SUMMARY

A cavity-stabilized XFELO using nuclear resonance, NRS-XFELO, will vastly improve its coherence properties of an XFELO and thus its science reach. Realizing a NRS-XFELO appears to be within the current state of the art, at least with ^{57}Fe resonance. Extending the stabilization to narrower resonances by an order of magnitude should also be feasible. NRS-XFELOs for even narrower resonances will be quite challenging but worthwhile, as they provide new scientific techniques hitherto not available in hard x-ray wavelengths, with applications in fundamental physics such as matter-wave interferometry and the study of how decoherence emerges in mesoscopic systems.

ACKNOWLEDGMENTS

We thank Jörg Evers for helpful discussions on quantum-optical applications of the XFELO. This work was supported by the U.S. Department of Energy, Office of Basic Energy Sciences under Contract No. DE-AC02-06CH11357.

APPENDIX A: THE ENSEMBLE AVERAGE OF PHASE NOISE

In order to evaluate the ensemble average in Eq. (14), several simplifications and approximations will now be applied. First, the sum over $n = 0 \ldots N-1, m = 0 \ldots N-1, n \neq m$ can be rewritten as one over $n = 1 \ldots N-1, m = 0 \ldots n-1$ plus its complex conjugate (c.c.). Equation (14) then becomes

$$U = 1 + \frac{1}{N} \sum_{n=0}^{N-1} \sum_{m=0}^{n-1} e^{i\omega(n-m)T_c} \left\langle e^{i(\psi_n - \psi_m)} \right\rangle + \text{c.c.}, \quad \text{(A1)}$$

where the complex conjugation refers to the double sum only.

As discussed above, the phases $\psi_n - \psi_m$ contain contributions from spontaneous undulator emission and cavity-length fluctuations at many different time scales. Because the x-ray pulses interact with the sources of phase noise (mirrors and electron beam) only at discrete times, $\psi_n - \psi_m$ may be represented as a sum $\phi_{n+1} + \phi_{n+2} \ldots \phi_m$ over discrete phase jumps. Each of these contains contributions from uncorrelated causes at different time scales. We may thus write

$$\psi_n - \psi_m = \sum_{q=1}^{(n-m)/2} \sum_{k=(m/q)+1}^{n/q} q\phi_{k,q}, \tag{A2}$$

where $\phi_{k,q}$ is the phase accumulated per turn due to a cause that lasts for q turns. For large $n, m, n-m$, all quotients $n/q, m/q, (n-m)/q$ can be considered as integers. The variance of the phases $\phi_{k,q}$ is now denoted as σ_q^2. Then, $q\phi_{k,q}$ has a variance of $q^2\sigma_q^2$, and the sum over $(n-m)/q$ terms has a variance of $q(n-m)\sigma_q^2$. Therefore, the variance of the phase fluctuations can be expressed as

$$\langle (\psi_n - \psi_m)^2 \rangle = (n-m) \sum_{q=1}^{(n-m)/2} q\sigma_q^2. \tag{A3}$$

If the series of σ_q approaches zero faster than q^{-2}, then the sum converges for $n - m \to \infty$. This is not the case in a passive cavity; in fact, longer-time-scale ground motion typically has a larger variance. However, the cavity-length control of the feedback loop will enforce that convergence by suppressing σ_q for $q > q_{\mathrm{FB}}$, where q_{FB} will be determined below:

$$\langle (\psi_n - \psi_m)^2 \rangle \approx (n-m) \sum_{q=1}^{\infty} q\sigma_q^2 =: (n-m)\sigma^2, \tag{A4}$$

which defines σ^2.

For a comb to exist at all, the phase differences must be small, i.e., $\psi_n - \psi_m \ll \pi$ for all n, m. Then, $\exp[i(\psi_n - \psi_m)] \approx 1 + i(\psi_n - \psi_m) - (\psi_n - \psi_m)^2/2$. The linear term has an ensemble average of zero, and, by Eq. (A4), the quadratic term can be replaced with $(n-m)\sigma^2$. Thus, $\langle \exp(\psi_n - \psi_m) \rangle$ in Eq. (A5) becomes $\exp[-(n-m)\sigma^2]$. Equation (A5) becomes now

$$U = 1 + \frac{1}{N} \sum_{n=0}^{N-1} \sum_{m=0}^{n-1} e^{i\omega(n-m)T_c} e^{-(n-m)\sigma^2} + \text{c.c.} \tag{A5}$$

The double sum has the form of

$$S(z) = \frac{1}{N} \sum_{n=0}^{N-1} \sum_{m=0}^{n-1} e^{-z(n-m)}, \qquad z = x + iy, \tag{A6}$$

with $z = \sigma^2/2 + i\omega T$. This becomes

$$S(z) = \frac{N(e^z - 1) + e^{(1-N)z} - e^z}{N(e^z - 1)^2}, \tag{A7}$$

which can be split as

$$S(z) = \frac{1}{e^z - 1} + \frac{e^{-Nz} - 1}{Ne^{-z}(e^z - 1)^2}. \tag{A8}$$

$S(z = x + iy)$ has peaks at $y = 2\pi n$ for integer n. In the most relevant case of $x \ll 1$ and $Nx \gg 1$, the contribution of the second term in Eq. (A8) to the peak becomes negligible. This can be seen by inserting the first-order expansion of the exponential where appropriate, i.e., $e^z - 1 \approx z$, but $e^{-Nz} \approx 0$:

$$S(z) \approx \frac{1}{x + iy} + \frac{-1}{Ne^{-z}(x + iy)^2}. \tag{A9}$$

The first fraction peaks up to $1/x$, while the absolute value of the second fraction peaks up to $1/Nx^2$, which is smaller than the first for $N \gg 1/x$. Besides being smaller, the second term also has a narrower peak due to the square in the denominator.

We proceed with the full Eq. (A8). After expanding the first fraction with $\exp(-z/2)$ and adding and subtracting $(e^{z/2} - e^{-z/2})/2(e^{z/2} - e^{-z/2})$, this becomes

$$S(z) = \underbrace{\frac{1}{2} \frac{e^{z/2} + e^{-z/2}}{e^{z/2} - e^{-z/2}}}_{S_{\mathrm{I}}} - \frac{1}{2} + \underbrace{\frac{e^{-Nz} - 1}{N(e^{z/2} - e^{-z/2})^2}}_{S_{\mathrm{II}}}. \tag{A10}$$

Expanding the first fraction with $e^{z^*/2} - e^{-z^*/2}$ then leads to

$$S_{\mathrm{I}}(z) = \frac{1}{4} \frac{\sinh x - i \sin y}{\sinh^2(x/2) + \sin^2(y/2)}. \tag{A11}$$

The third fraction in Eq. (A10) can be expanded with $(e^{z^*/2} - e^{-z^*/2})^2$ to yield

$$S_{\mathrm{II}}(z) = \frac{(e^{-Nz} - 1)(e^{z^*/2} - e^{-z^*/2})^2}{N|e^{z/2} - e^{-z/2}|^2}, \tag{A12}$$

which, after some algebraic steps, becomes

$$S_{\mathrm{II}}(z) = \frac{2 - e^{z^*} - e^{-z^*} + e^{-Nz}(e^{z^*} + e^{-z^*} - 2)}{16N[\sinh^2(x/2) + \sin^2(y/2)]^2}. \tag{A13}$$

After some further algebraic steps, and with the introduction of

$$C_N(x,y) = \frac{e^x \cos[(N+1)y] + e^{-x}\cos[(N-1)y]}{2} - \cos(Ny) \tag{A14}$$

and

$$S_N(x,y) = -\frac{e^x \sin[(N+1)y] + e^{-x}\cos[(N-1)y]}{2} - \sin(Ny), \tag{A15}$$

we arrive at

$$S_{\mathrm{II}}(x+iy) = \frac{1-\cosh x\cos y + e^{-Nx}C_N(x,y)}{8N[\sinh^2(x/2)+\sin^2(y/2)]^2} + i\frac{\sinh x\sin y + e^{-Nx}S_N(x,y)}{8N[\sinh^2(x/2)+\sin^2(y/2)]^2}. \tag{A16}$$

Inserting Eqs. (A11) and (A16) into (A10), and that into (A5), we arrive at

$$U = \frac{\sinh(\sigma^2/2)}{\sinh^2(\sigma^2/4)+\sin^2(\omega T/2)} + \frac{1-\cosh(\sigma^2/2)\cos(\omega T) + e^{-N\sigma^2/2}C_N(\sigma^2/2,\omega T)}{4N[\sinh^2(\sigma^2/4)+\sin^2(\omega T/2)]^2}. \tag{A17}$$

Note that the imaginary parts in (A11) and (A16) cancel out in the complex conjugation of (A5).

APPENDIX B: THE XFELO COMB

This Appendix contains a brief discussion of the properties of the laser cavity in comparison to a Fabry-Perot interferometer. The intracavity modes differ from those of a passive Fabry-Perot interferometer (FPI) in that the laser gain compensates for loss in a few (ideally, one) transverse modes. The spectrum observed in the output has the typical comb structure, but the linewidths of the modes with laser gain are not given by the finesse. Rather, they are determined by random phase-shifting influences, such as spontaneous-emission noise, or cavity-length fluctuations. The cross section of the gain medium—here the electron beam in the undulator—naturally provides a spatial filter that selects one or a few spatial modes, while all other modes are those of a passive FPI, subject to exponential decay. If the cavity remains stable, then successive pulses have well-defined phases to each other. In a sample with a sufficiently narrow-band response, such as a nuclear resonance, interference of pulses with the lingering effects from preceding pulses makes sharp spectral features like a comb apparent. However, absent such a narrow-band filter, there are no physical effects inside the cavity that could be attributed to the phase coherence of successive pulses or the corresponding comblike spectrum.

[1] B. W. Adams *et al.*, J. Mod. Opt. **60**, 2 (2013).
[2] M. O. Scully and M. S. Zubairy, *Quantum Optics* (Cambridge University Press, Cambridge, England, 1997).
[3] R. Röhlsberger, K. Schlage, B. Sahoo, S. Couet, and R. Rüffer, Science **328**, 1248 (2010).
[4] R. Röhlsberger, H.-C. Wille, K. Schlage, and B. Sahoo, Nature (London) **482**, 199 (2012).
[5] R. Colella and A. Luccio, Opt. Commun. **50**, 41 (1984).
[6] K.-J. Kim, Y. Shvydko, and S. Reiche, Phys. Rev. Lett. **100**, 244802 (2008).
[7] K.-J. Kim and Y. V. Shvyd'ko, Phys. Rev. ST Accel. Beams **12**, 030703 (2009).
[8] R. R. Lindberg, K.-J. Kim, Yu. Shvydko, and W. M. Fawley, Phys. Rev. ST Accel. Beams **14**, 010701 (2011).
[9] R. Bonifacio, C. Pellegrini, and L. M. Narducci, Opt. Commun. **50**, 373 (1984).
[10] P. Emma, for the LCLS commissioning team, First lasing of the LCLS x-ray FEL at 1.5 Å (unpublished).
[11] G. Geloni, V. Kocharyan, and E. Saldin, J. Mod. Opt. **58**, 1391 (2011).
[12] J. Amann *et al.*, Nat. Photonics **6**, 693 (2012).
[13] C. Brau, *Free-Electron Lasers* (Academic Press, New York, 1990).
[14] H. Al-Abawi, F. A. Hoff, G. T. Moore, and M. O. Scully, Opt. Commun. **30**, 235 (1979).
[15] S. T. Cundiff and J. Ye, Rev. Mod. Phys. **75**, 325 (2003).
[16] S. Whitcomb (private communication).
[17] S. Stoupin, F. Lenkszus, R. Laird, K. Goetze, K.-J. Kim, and Y. Shvydko, Rev. Sci. Instrum. **81**, 055108 (2010).
[18] W.-T. Liao, S. Das, C. H. Keitel, and A. Palffy, Phys. Rev. Lett. **109**, 262502 (2012).
[19] S. Stoupin and Y. V. Shvydko, Phys. Rev. Lett. **104**, 085901 (2010).
[20] S. Stoupin and Y. V. Shvydko, Phys. Rev. B **83**, 104102 (2011).
[21] G. V. Smirnov, Hyperfine Interact. **123-124**, 31 (1999).
[22] Saulson, http://cgwa.phys.utb.edu/Files/Events/29_630_Saulson_0614_Vibration_Isolation.pdf.
[23] Y. V. Shvyd'ko, *X-Ray Optics*, Springer Series in Optical Sciences (Springer, New York, 2004).
[24] Zygo Corporation, Laser interferometers, (2014), http://www.zygo.com/?/met/interferometers/.
[25] Keysight Technologies (formerly Agilent), Laser interferometer position measurement systems, (2014), www.agilent.com.
[26] H. Fraunfelder, *The Mössbauer Effect* (Benjamin, New York, 1963).
[27] D. Vitali, S. Gigan, A. Ferreira, H. R. Böhm, P. Tombesi, A. Guerreiro, V. Vedral, A. Zeilinger, and M. Aspelmeyer, Phys. Rev. Lett. **98**, 030405 (2007).

[28] K. P. Heeg *et al.*, Phys. Rev. Lett. **111**, 073601 (2013).
[29] B. W. Adams and K.-J. Kim, *ICFA Newsletter* **60**, 56 (2013).
[30] O. Romero-Isart, A. C. Pflanzer, F. Blaser, R. Kaltenbaek, N. Kiesel, M. Aspelmeyer, and J. I. Cirac, Phys. Rev. Lett. **107**, 020405 (2011).
[31] P. Kok, H. Lee, and J. P. Dowling, Phys. Rev. A **65**, 052104 (2002).
[32] M. W. Mitchell, J. S. Lundeen, and A. M. Steinberg, Nature (London) **429**, 161 (2004).
[33] I. Afek, O. Ambar, and Y. Silverberg, Science **328**, 879 (2010).